ARTICLE

doi:10.1038/nature10137

Role of YAP/TAZ in mechanotransduction

Sirio Dupont[1]*, Leonardo Morsut[1]*, Mariaceleste Aragona[1], Elena Enzo[1], Stefano Giulitti[2], Michelangelo Cordenonsi[1], Francesca Zanconato[1], Jimmy Le Digabel[3], Mattia Forcato[4], Silvio Bicciato[4], Nicola Elvassore[2] & Stefano Piccolo[1]

Cells perceive their microenvironment not only through soluble signals but also through physical and mechanical cues, such as extracellular matrix (ECM) stiffness or confined adhesiveness. By mechanotransduction systems, cells translate these stimuli into biochemical signals controlling multiple aspects of cell behaviour, including growth, differentiation and cancer malignant progression, but how rigidity mechanosensing is ultimately linked to activity of nuclear transcription factors remains poorly understood. Here we report the identification of the *Yorkie*-homologues YAP (Yes-associated protein) and TAZ (transcriptional coactivator with PDZ-binding motif, also known as WWTR1) as nuclear relays of mechanical signals exerted by ECM rigidity and cell shape. This regulation requires Rho GTPase activity and tension of the actomyosin cytoskeleton, but is independent of the Hippo/LATS cascade. Crucially, YAP/TAZ are functionally required for differentiation of mesenchymal stem cells induced by ECM stiffness and for survival of endothelial cells regulated by cell geometry; conversely, expression of activated YAP overrules physical constraints in dictating cell behaviour. These findings identify YAP/TAZ as sensors and mediators of mechanical cues instructed by the cellular microenvironment.

Physical properties of the extracellular matrix (ECM) and mechanical forces are integral to morphogenetic processes in embryonic development, defining tissue architecture and driving specific cell differentiation programs[1]. In adulthood, tissue homeostasis remains dependent on physical cues, such that perturbations of ECM stiffness—or mutations affecting its perception—are causal to pathological conditions of multiple organs, contributes to ageing and cancer malignant progression[2].

Mechanotransduction enables cells to sense and adapt to external forces and physical constraints[3,4]; these mechanoresponses involve the rapid remodelling of the cytoskeleton, but also require the activation of specific genetic programs. In particular, variations of ECM stiffness or changes in cell shape caused by confining the cell's adhesive area have a profound impact on cell behaviour across several cell types, such as mesenchymal stem cells[5,6], muscle stem cells[7] and endothelial cells[8]. The nuclear factors mediating the biological response to these physical inputs remain incompletely understood.

ECM stiffness regulates YAP/TAZ activity

To gain insight into these issues, we asked if physical/mechanical stimuli conveyed by ECM stiffness actually signal through known signalling pathways. For this, we performed a bioinformatic analysis on genes differentially expressed in mammary epithelial cells (MEC) grown on ECM of high versus low stiffness[9]. Specifically, we searched for statistical associations between genes regulated by stiffness and gene signatures denoting the activation of specific signalling pathways (Supplementary Fig. 2, Supplementary Table 1 and Methods). We included signatures of MAL/SRF and NF-κB as these factors translocate in the nucleus in response to changes in F-actin polymerization and cell stretching[10]. Strikingly, only signatures revealing activation of YAP/TAZ transcriptional regulators emerged as significantly overrepresented in the set of genes regulated by high stiffness (Supplementary Fig. 2).

To test if YAP and TAZ activity is regulated by ECM stiffness, we monitored YAP/TAZ transcriptional activity in human MEC grown on fibronectin-coated acrylamide hydrogels of varying stiffness (elastic modulus ranging from 0.7 to 40 kPa, matching the physiological elasticities of natural tissues[6]). For this, we assayed by real-time PCR two of the best YAP/TAZ regulated genes from our signature, *CTGF* and *ANKRD1*. The activity of YAP/TAZ in cells grown on stiff hydrogels (15–40 kPa) was comparable to that of cells grown on plastics, whereas growing cells on soft matrices (in the range of 0.7–1 kPa) inhibited YAP/TAZ activity to levels comparable to short interfering RNA (siRNA)-mediated YAP/TAZ depletion (Fig. 1a and data not shown). We confirmed this finding in other cellular systems, such as MDA-MB-231 and HeLa cells, where we used a synthetic YAP/TAZ-responsive luciferase reporter (4×GTIIC-lux) as direct read-out of their activity (Fig. 1a and Supplementary Fig. 4).

Next, we assayed endogenous YAP/TAZ subcellular localization; indeed, their cytoplasmic relocalization has been extensively used as primary read-out of their inhibition by the Hippo pathway or by cell–cell contact (Supplementary Fig. 5 and ref. 11). By immunofluorescence on MEC and human mesenchymal stem cells (MSC, an established non-epithelial cellular model for mechanoresponses[5,6]), YAP/TAZ were clearly nuclear on hard substrates but became predominantly cytoplasmic on softer substrates (Fig. 1b and Supplementary Figs 6 and 7). Collectively, these data indicate that YAP/TAZ activity and subcellular localization are regulated by ECM stiffness.

YAP/TAZ are regulated by cell geometry

It is recognized that changes in ECM stiffness impose different degrees of cell spreading[6,12]. We thus asked whether cell spreading is sufficient to regulate YAP/TAZ. To this end, we used micropatterned fibronectin 'islands' of defined size, on which cells can spread to different degrees depending on the available adhesive area[8]. On these micropatterns, the localization of YAP/TAZ changed from predominantly nuclear in spread MSCs, to predominantly cytoplasmic in cells on smaller islands (Fig. 1c). Of note, the use of single-cell adhesive islands rules out the possibility that cell–cell contacts could be involved in YAP/TAZ relocalization. We confirmed these results using human lung microvascular endothelial cells (HMVEC, Fig. 1d), that are well known to regulate their growth according to cell shape[8].

[1]Department of Histology, Microbiology and Medical Biotechnologies, University of Padua School of Medicine, viale Colombo 3, 35131 Padua, Italy. [2]Department of Chemical Engineering (DIPIC), University of Padua, via Marzolo 9, 35131 Padua, Italy. [3]Laboratoire Matière et Systèmes Complexes (MSC), Université Paris Diderot and CNRS UMR 7057, 10 rue A. Dumont et L. Duquet, 75205 Paris, France. [4]Center for Genome Research, Department of Biomedical Sciences, University of Modena and Reggio Emilia, via G. Campi 287, 41100 Modena, Italy.
*These authors contributed equally to this work.

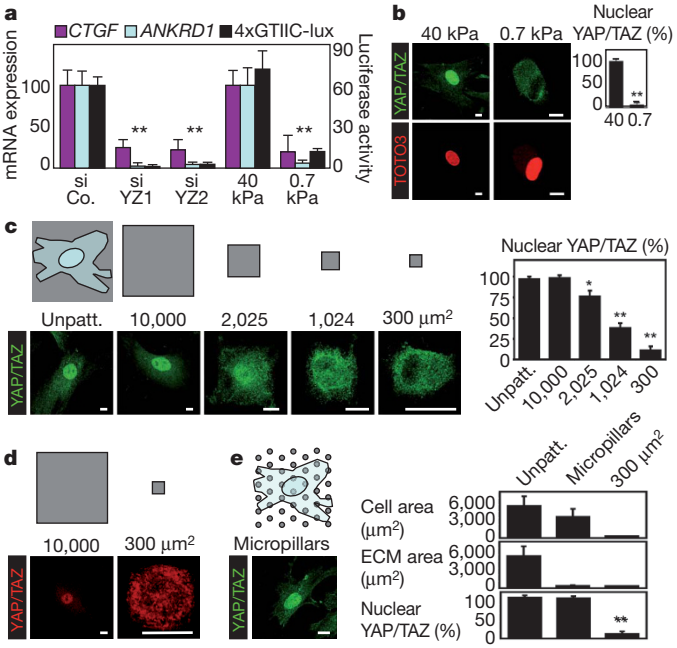

Figure 1 | YAP/TAZ are regulated by ECM stiffness and cell shape **a**, Real-time PCR analysis in MCF10A cells (*CTGF* and *ANKRD1*, coloured bars) and luciferase reporter assay in MDA-MB-231 cells (4×GTIIC-lux, black bars) to measure YAP/TAZ transcriptional activity. Cells were transfected with the indicated siRNAs (siCo., control siRNA; siYZ1 and siYZ2, two YAP/TAZ siRNAs; see Supplementary Fig. 3) and grown on plastic, or plated on stiff (elastic modulus of 40 kPa) and soft (0.7 kPa) fibronectin-coated hydrogels. Data are normalized to lane 1. $n = 4$. **b**, Confocal immunofluorescence images of YAP/TAZ and nuclei (TOTO3) in human mesenchymal stem cells (MSC) plated on hydrogels. Scale bars, 15 μm. Graphs indicate the percentage of cells with nuclear YAP/TAZ. ($n = 3$). **c**, On top: grey patterns show the relative size of microprinted fibronectin islands of decreasing sizes (μm²). Scale bars, 15 μm. Graph provides quantifications. ($n = 8$). See also Supplementary Fig. 8. **d**, Confocal immunofluorescence images of YAP/TAZ in HMVEC plated as in **c**. Scale bars, 15 μm. See also Supplementary Fig. 9. **e**, On top: grey dots exemplify the distribution of fibronectin on micropillar arrays, shown superimposed with the outline of a cell. Below: representative immunofluorescence of YAP/TAZ in MSC plated on rigid micropillars. Scale bars, 15 μm. Graphs, quantification of the projected cell area, total ECM contact area, and nuclear YAP/TAZ in MSC plated on unpatterned fibronectin, micropillars and 300 μm² islands. ($n = 4$). All error bars are s.d. (*$P < 0.05$; **$P < 0.01$; Student's *t*-test is used throughout). Experiments were repeated *n* times with duplicate biological replicates.

Cells seeded on stiff hydrogels or large islands show increased cell spreading but, at the same time, experience a broader cell–ECM contact area. To test whether YAP/TAZ are regulated by cell spreading irrespectively of the total amount of ECM, we visualized YAP/TAZ localization in MSC grown on the tip of closely arrayed fibronectin-coated micropillars[12]: on these arrays, cells stretch from one micropillar to another, and assume a projected cell area comparable to cells plated on big islands (3,200 μm² on average, Fig. 1e); however, in these conditions, the actual area available for cell–ECM interaction is only about 10% of their projected area (300 μm² on average, corresponding to the smallest islands used in Fig. 1c). YAP/TAZ remained nuclear on micropillars (Fig. 1e), indicating that YAP/TAZ are primarily regulated by cell spreading imposed by the ECM.

YAP/TAZ sense cytoskeletal tension

We then considered that cell spreading entails activation of the small GTPase Rho that, in turn, regulates the formation of actin bundles, stress fibres and tensile actomyosin structures[2,3]. Indeed, cells on stiff ECM or big islands had more prominent stress fibres compared to those plated on soft ECM or small islands (Supplementary Figs 9 and 10). As shown in Fig. 2a, we found that Rho and the actin cytoskeleton are required to maintain nuclear YAP/TAZ in MSC. As a control, inhibition of Rac1-GEFs (guanine nucleotide exchange factors), or disruption of microtubules, did not alter YAP/TAZ localization (Fig. 2a). Similar results were obtained also in HMVEC and MEC (not shown). Crucially, inhibition of Rho and of the actin cytoskeleton also inhibited YAP/TAZ transcriptional activity, as assayed by expression of endogenous target genes (Fig. 2b) and by luciferase reporter assays (Fig. 2c). Conversely, triggering F-actin polymerization and stress fibres formation by overexpression of activated diaphanous protein (*DIAPH1*) promoted YAP/TAZ activity (Supplementary Fig. 12).

We then asked whether YAP/TAZ are regulated by the ratio of monomeric/filamentous actin, as others observed for MAL/SRF[13]. To increase monomeric G-actin, we overexpressed the R62D mutant actin[13], but this was insufficient to inhibit YAP/TAZ (Fig. 2c). Moreover, increasing the amount of F-actin either by overexpressing the F-actin stabilizing V159N actin mutant or by serum stimulation[13] had no effect on YAP/TAZ activity (Supplementary Fig. 13) or nuclear localization (data not shown). As a control, in the same experimental set-up, MAL/SRF activity was instead clearly modulated

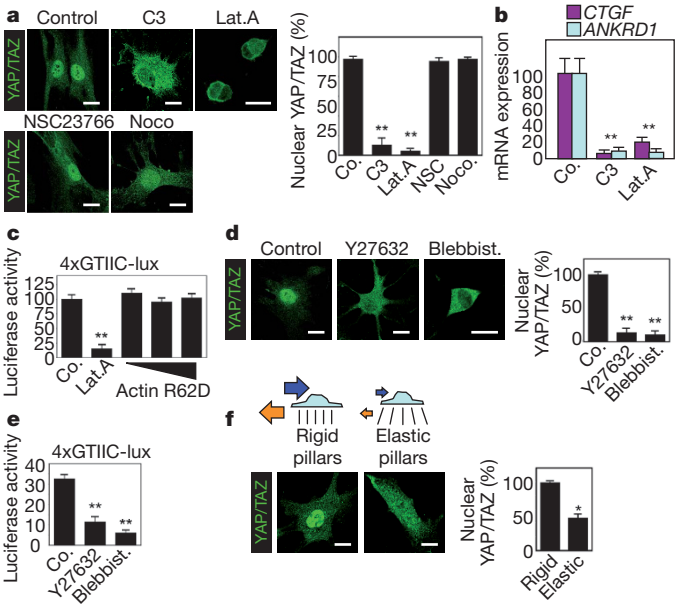

Figure 2 | YAP/TAZ activity requires Rho and tension of the actin cytoskeleton **a**, Confocal immunofluorescence images of YAP/TAZ in MSC treated with the Rho inhibitor C3 (3 μg ml^{-1}), the F-actin inhibitor latrunculin A (Lat.A, 0.5 μM), the Rac1-GEFs inhibitor NSC23766 (100 μM) or the microtubule inhibitor nocodazole (Noco., 30 μM). Scale bars, 15 μm. Graph provides quantifications ($n = 10$). See also Supplementary Fig. 11. **b**, Real-time PCR of MCF10A treated with cytoskeletal inhibitors as in **a**. Data are normalized to untreated cells (Co.) ($n = 4$). **c**, Luciferase assay for YAP/TAZ activity in HeLa cells transfected with the indicated expression plasmids (Co. is empty vector, actin R62D encodes for a mutant unable to polymerize into F-actin) and treated with latrunculin A ($n = 4$). Similar effects were observed in MDA-MB-231 (not shown). **d**, Confocal immunofluorescence images of MSC treated with the ROCK inhibitor Y27632 (50 μM), or the non-muscle myosin inhibitor blebbistatin (Blebbist., 50 μM). Scale bars, 15 μm. Graph provides quantifications ($n = 9$). See also Supplementary Fig. 15. **e**, Luciferase activity of the YAP/TAZ reporter in HeLa treated as in **d**. ($n = 4$). **f**, Confocal immunofluorescence images of MSC plated on arrays of micropillars of different rigidities. On rigid micropillars (black lines) cells develop cytoskeletal tension (blue arrow) by pulling against the ECM (orange arrow); cells bend elastic micropillars and develop reduced tension exemplified by reduced size of the arrows. Scale bars, 15 μm. Graph provides quantifications ($n = 2$). See also Supplementary Fig. 19. All error bars are s.d. (*$P < 0.05$; **$P < 0.01$). Experiments were repeated *n* times with duplicate biological replicates.

(Supplementary Fig. 14). Taken altogether, these data indicate that Rho and stress fibres, but not F-actin polymerization *per se*, are required for YAP/TAZ activity.

Cells respond to the rigidity of the ECM by adjusting the tension and organization of their stress fibres, such that cell spreading is accompanied by increased pulling forces against the ECM[3,6,12]. By inhibition of ROCK and non-muscle myosin[4,6], we found that cytoskeletal tension is required for YAP/TAZ nuclear localization (Fig. 2d) and activity (Fig. 2e and Supplementary Fig. 16). Of note, YAP/TAZ exclusion caused by these inhibitions is an early event (occurring within 2 h) that can be uncoupled from destabilization of stress fibres (see Supplementary Fig. 17). By comparison, the activity of MAL/SRF was only marginally affected by the same treatments (Supplementary Fig. 18). To address more directly the relevance of cell-generated mechanical force without using small-molecule inhibitors and irrespectively of the surface properties of the hydrogels, we compared rigid versus highly elastic micropillars[12]; on the elastic substrate, cytoplasmic localization of YAP/TAZ was clearly increased (Fig. 2f). Collectively, the data indicate that YAP/TAZ respond to cytoskeletal tension.

We also tested if inhibition of YAP/TAZ occurs by entrapping YAP/TAZ in the cytoplasm or by promoting their nuclear exclusion. As shown in Supplementary Fig. 20a, blockade of nuclear export with leptomycin B rescued nuclear localization of YAP/TAZ in MSC treated with cytoskeletal inhibitors, indicating that YAP/TAZ keeps shuttling between cytoplasm and nucleus irrespectively of cell tension, and that the presence of a tense cytoskeleton promotes their nuclear retention. Moreover, YAP/TAZ relocalization was rapid (occurring in as little as 30 min with latrunculin A), reversible after small-molecule washout (Supplementary Fig. 20b), and insensitive to inhibition of protein synthesis with cycloheximide (data not shown), suggesting a direct biochemical mechanism.

Mechanical cues act independently from Hippo

YAP and TAZ are the nuclear transducers of the Hippo pathway[14]. In several organisms and cellular set-ups, activation of the Hippo pathway leads to YAP/TAZ phosphorylation on specific serine residues; in turn, these phosphorylations inhibit YAP/TAZ activity through multiple mechanisms, including proteasomal degradation[14]. Intriguingly, similar to Hippo activation by cell–cell contacts (Fig. 3a), TAZ protein was also degraded by growing MEC on soft matrices (Fig. 3b) or by treatment with inhibitors of Rho, F-actin and actomyosin tension (Fig. 3c and Supplementary Fig. 21). Similar results were obtained with MSC and HMVEC (Supplementary Fig. 22 and data not shown).

Is then the Hippo cascade responsible for YAP/TAZ inhibition by mechanical cues? Several evidences indicate this is not the case. First, we noted that phosphorylation of YAP on serine 127, a key target of the LATS kinase downstream of the Hippo pathway[15], was not increased upon treatment of MEC and MSC with cytoskeletal inhibitors (Fig. 3c and Supplementary Fig. 22), at difference with its regulation by high confluence (see Fig. 3a). Second, depletion of LATS1 and LATS2 (see Fig. 3f and Supplementary Fig. 23 for positive controls) had marginal effect on YAP/TAZ inactivation by mechanical cues, as judged by (1) YAP/TAZ nuclear exit induced by micropatterns or cytoskeletal inhibition in MEC, MSC or HMVEC (Fig. 3d and Supplementary Figs 24, 25 and data not shown); (2) TAZ degradation (Fig. 3e); (3) endogenous target gene expression in cells plated on soft hydrogels (Fig. 3f) or treated with latrunculin A (Supplementary Fig. 26). Finally, we compared wild-type or LATS-insensitive 4SA[16] TAZ in MDA-MB-231 depleted of endogenous YAP/TAZ and reconstituted at near-to-endogenous YAP/TAZ activity levels with siRNA-insensitive mouse TAZ vectors. As shown in Fig. 3g, both wild-type and 4SA TAZ remain sensitive to mechanical cues. Further supporting these results, we found that MDA-MB-231 cells are homozygous mutant for NF2 (also known as merlin, Supplementary Fig. 27), an essential component of the Hippo cascade[14]. Collectively, these data indicate that LATS phosphorylation downstream of the Hippo cascade is not the primary mediator of mechanical/physical cues in regulating YAP/TAZ activity.

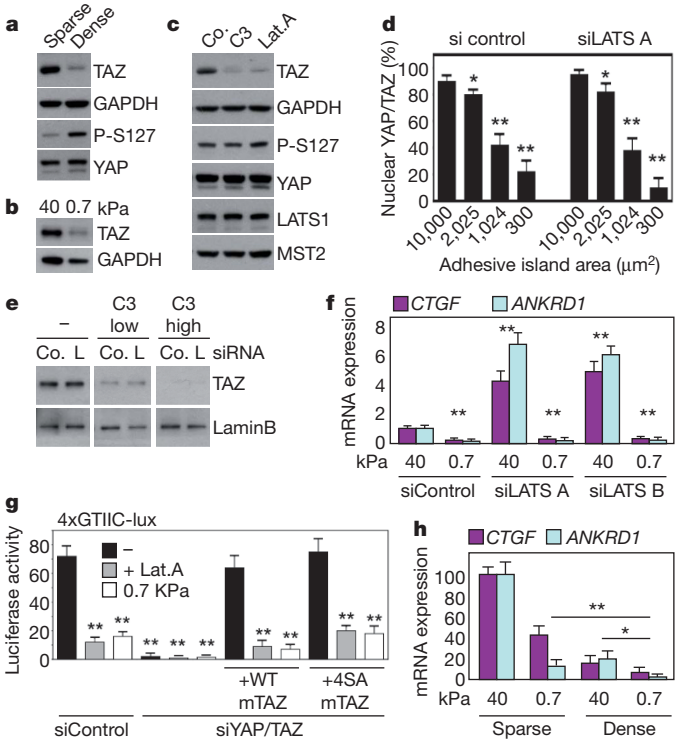

Figure 3 | ECM stiffness and cell spreading regulate YAP/TAZ independently of the Hippo pathway **a**–**c**, Immunoblotting for the indicated proteins in MCF10A under the following conditions: **a**, plating on plastic at low (sparse) or high (dense) confluence; **b**, plating on stiff (40 kPa) or soft (0.7 kPa) hydrogels; **c**, untreated (Co.) or treated with C3 and latrunculin A (Lat.A). P-S127 is phospho-YAP. **d**, Quantification of nuclear YAP/TAZ in MSC transfected with control or LATS1/2 siRNA A (siLATS A) and plated on microprinted islands of different size ($n = 4$). Similar results were obtained with HMVEC (not shown). **e**, Immunoblotting from MSC cells transfected with the indicated siRNAs (Co., control siRNA; L, LATS1/2 siRNA A), plated on plastic and treated with C3 (0.5 or 3 μg ml^{-1}). Similar results were obtained by using blebbistatin or latrunculin A, or by treating HMVEC and MCF10A (not shown). **f**, Real-time PCR analysis of MCF10A transfected with the indicated siRNAs and cultured on hydrogels. Data are normalized to the first lane ($n = 3$). **g**, Luciferase assay in MDA-MB-231 transfected as indicated and treated with latrunculin A (Lat.A) or replated on soft hydrogels. ($n = 8$). **h**, RT–PCR of MCF10A grown under sparse or confluent (dense) conditions on the indicated hydrogels. Data are normalized to the first lane ($n = 2$). All error bars are s.d. ($^*P < 0.05$; $^{**}P < 0.01$). Experiments were repeated n times with duplicate biological replicates.

We then asked if mechanical cues regulate YAP/TAZ not only in isolated cells, but also in confluent monolayers, when cells reorganize their shape and structure and engage in cell–cell contacts, leading to activation of Hippo/LATS signalling[11]. We first explored the effects of cell confluence in a simplified experimental set-up, namely in MCF10A cells rendered insensitive to Hippo activation by depletion of LATS1/2; in these conditions, Rho and the cytoskeleton remain relevant inputs to support TAZ stability (Supplementary Fig. 28). Moreover, in parental MCF10A, plating cells at high confluence cooperate with soft hydrogels in inhibiting YAP/TAZ activity (Fig. 3h). Thus, mechanical cues and Hippo signalling represent two parallel inputs converging on YAP/TAZ regulation.

YAP/TAZ mediate cellular mechanoresponses

Data presented so far indicate YAP and TAZ as molecular 'readers' of ECM elasticity and cell geometry, but are YAP/TAZ relevant to mediate the biological responses to these mechanical inputs? An appropriate

cellular model to address this question are MSC, that can differentiate into osteoblasts when cultured on stiff ECM, mimicking the natural bone environment, whereas on soft ECM—or small islands—they differentiate into other lineages, such as adipocytes[5,6]. A similar case applies to endothelial cells, that respond differently to the same soluble growth factor by proliferating, differentiating or involuting according to the degree of cell spreading against the surrounding ECM[8]. We proposed that cell fates induced by stiff ECM and large islands (that is, where YAP/TAZ are active) should require YAP/TAZ function and, conversely, cell fates associated to soft ECM and small islands (where YAP/TAZ are inhibited) should require their inactivation. In line with this hypothesis, osteogenic differentiation induced in MSC on stiff ECM was inhibited upon depletion of YAP and TAZ, and a similar inhibition was achieved either by culturing cells on soft ECM or by incubation with C3 (Fig. 4a, b). We also monitored adipogenic differentiation, a fate normally not allowed on stiff ECM; strikingly, YAP/TAZ knockdown enabled adipogenic differentiation on stiff substrates, thus mimicking a soft environment (Fig. 4c and Supplementary Fig. 30). In the case of HMVEC, cells plated on small islands undergo apoptosis, whereas cells on bigger islands proliferate, as assayed by TdT-mediated dUTP nick end labelling (TUNEL) staining and 5-bromodeoxyuridine (BrdU) incorporation, respectively[8]. Upon YAP/TAZ depletion, cells on bigger islands behaved as if they were on small islands; this is overlapping with the biological effects of Rho inhibition (Fig. 4d). In line with the Hippo independency of this regulation, knockdown of LATS1/2 was not sufficient to rescue osteogenesis upon C3 treatment, or endothelial cell proliferation on small islands (Supplementary Fig. 32). Collectively, these data suggest that YAP/TAZ are required for cell differentiation triggered by changes in ECM stiffness and for geometric control of cell survival.

We next tested if the sole YAP/TAZ activity can re-direct the biological responses elicited by soft/confined ECM. Overexpression of activated 5SA-YAP (ref. 14) with lentiviral infection (to at least ten-fold the endogenous levels, data not shown) remarkably overruled the geometric control over proliferation and apoptosis in HMVEC (Fig. 4e), and rescued osteogenic differentiation of MSC treated with C3 or plated on soft ECM (Fig. 4f, g). Thus, cells on soft matrices or on small adhesive areas can be 'tricked' to behave as if they were adhering on harder/larger substrates by sustaining YAP/TAZ function.

Discussion

In summary, our findings indicate a fundamental role of the transcriptional regulators YAP and TAZ as downstream elements in how cells perceive their physical microenvironment (Supplementary Fig. 1). Our data define an unprecedented modality of YAP/TAZ regulation, that acts in parallel to the NF2/Hippo/LATS pathway, and instead requires Rho activity and the actomyosin cytoskeleton. Interestingly, this recapitulates aspects of MAL/SRF regulation[13], but also entails profound differences: YAP/TAZ activity requires stress fibres and cytoskeletal tension induced by ECM stiffness and cell spreading, but is not directly regulated by G-actin levels. The detailed biochemical mechanisms by which cytoskeletal tension regulates YAP/TAZ await further characterization, but it is tempting to speculate that stress-fibres inhibit an unidentified YAP/TAZ-antagonist. Functionally, we showed in different cellular models that cells read ECM elasticity, cell shape and cytoskeletal forces as levels of YAP/TAZ activity, such that experimental manipulations of YAP/TAZ levels can dictate cell behaviour, overruling mechanical inputs. This identifies a new widespread transcriptional mechanism by which the mechanical properties of the ECM and cell geometry instruct cell behaviour. This may now shed light on how physical forces shape tissue morphogenesis and homeostasis, for example in tissues undergoing constant remodelling upon variation of their mechanical environment; indeed, alterations of YAP/TAZ signalling have been genetically linked in animal models to the emergence of cystic kidney, pulmonary emphysema, heart and vascular defects[17–20]. In cancer, changes in the ECM composition and

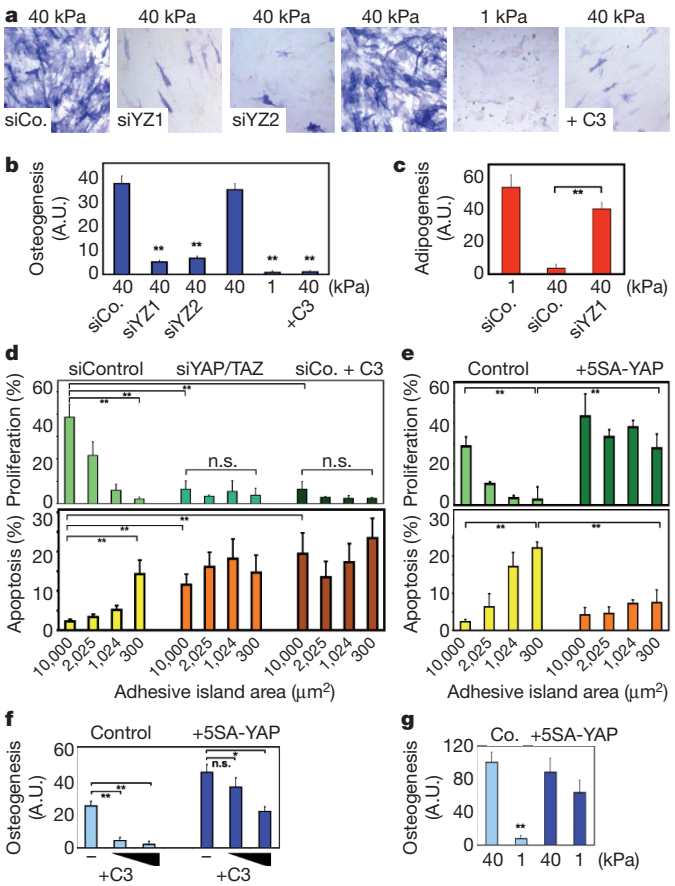

Figure 4 | YAP/TAZ are required mediators of the biological effects controlled by ECM elasticity and cell geometry **a**–**c**, MSC were transfected with the indicated siRNA (control, siCo.; YAP/TAZ, siYZ1 and siYZ2), plated on stiff (40 kPa) or soft (1 kPa) substrates and induced to differentiate into osteoblasts (**a**, **b**) or adipocytes (**c**). C3 (0.5 μg ml^{-1}) was added and renewed with differentiation medium. **a**, Representative alkaline phosphatase stainings and **b**, quantifications of osteogenic differentiation ($n = 4$). **c**, Quantification of adipogenesis based on oil-red stainings ($n = 2$) (A.U., arbitrary units, see methods). See Supplementary Figs 29 and 30 for controls. These results are consistent with ref. 23. **d**, Proliferation (BrdU, upper panel) and apoptosis (TUNEL, lower panel) of HMVEC plated on adhesive islands of different size; where indicated, cells were treated overnight with C3 (2.5 μg ml^{-1}), or transfected with the indicated siRNAs ($n = 5$). Similar results were obtained with siYZ2 (not shown). Representative stainings in Supplementary Fig. 31. **e**, Proliferation (upper panel) and apoptosis (lower panel) of control and 5SA-YAP-expressing HMVEC, plated on adhesive islands. **f**, **g**, Quantifications of osteogenesis in MSC transduced with 5SA-YAP, and treated with C3 (50 and 150 ng ml^{-1}) ($n = 3$) (**f**) or plated on hydrogels ($n = 2$) (**g**). Representative stainings in Supplementary Fig. 33. All error bars are s.d. (*$P < 0.05$; **$P < 0.01$; n.s., not significant). Experiments were repeated n times with duplicate biological replicates.

mechanical properties is the focus of intense interest, as these have been correlated with progression and build-up of the metastatic niche[2]; in light of their powerful oncogenic activities[14], YAP/TAZ might serve as executers of these malignant programs.

Genetically, YAP and TAZ have been linked to a universal system that controls organ size[14]. The current view implicates Hippo signalling as the sole determinant of YAP/TAZ regulation in tissues. However, our results suggest physical/mechanical inputs as alternative determinants of YAP/TAZ activity. Supporting this view, it has been observed that growth of epithelial tissues entails the build-up of mechanical stresses at tissue boundaries[21], and theoretical work proposed that these serve as positive feedback to homogenize cell growth, compensating for uneven activity of soluble growth factors[22]. It is tempting to speculate that proliferative tissue homeostasis may be

achieved by a combination of growth factor signalling and localized control of YAP/TAZ activation by cell–cell contacts and mechanical cues dictated by tissue architecture.

METHODS SUMMARY

MSC and HMVEC-L cells, their growth and differentiation media, were from Lonza. Micropatterned slides were from Cytoo SA. Micropost arrays and acrylamide hydrogels were synthesized according to standard procedures. Drug treatments were performed in 8-well Lab-Tek chamber slides (Nunc). Transfections were carried out with TransitLT1 (MirusBio) for plasmids, with Lipofectamine RNAiMax (Invitrogen) for siRNA (sequences in Supplementary Table 2). Anti-YAP/TAZ is sc101199 (SantaCruz). Other stainings were DeadEnd (Promega) for TUNEL, kit number 1 (Roche) for BrdU, kit number 85L2 (Sigma) for alkaline phosphatase, Oil-red (Sigma) for lipid vacuoles. Real-time PCR was performed on dT-primed cDNA with a RG3000 Corbett Research cycler (primers in Supplementary Table 3).

Full Methods and any associated references are available in the online version of the paper at www.nature.com/nature.

Received 3 November 2010; accepted 19 April 2011.

1. Mammoto, T. & Ingber, D. E. Mechanical control of tissue and organ development. *Development* **137,** 1407–1420 (2010).
2. Jaalouk, D. E. & Lammerding, J. Mechanotransduction gone awry. *Nature Rev. Mol. Cell Biol.* **10,** 63–73 (2009).
3. Schwartz, M. A. Integrins and extracellular matrix in mechanotransduction. *Cold Spring Harb. Perspect. Biol.* **2,** a005066 (2010).
4. Vogel, V. & Sheetz, M. Local force and geometry sensing regulate cell functions. *Nature Rev. Mol. Cell Biol.* **7,** 265–275 (2006).
5. McBeath, R., Pirone, D. M., Nelson, C. M., Bhadriraju, K. & Chen, C. S. Cell shape, cytoskeletal tension, and RhoA regulate stem cell lineage commitment. *Dev. Cell* **6,** 483–495 (2004).
6. Engler, A. J., Sen, S., Sweeney, H. L. & Discher, D. E. Matrix elasticity directs stem cell lineage specification. *Cell* **126,** 677–689 (2006).
7. Gilbert, P. M. *et al.* Substrate elasticity regulates skeletal muscle stem cell self-renewal in culture. *Science* **329,** 1078–1081 (2010).
8. Chen, C. S., Mrksich, M., Huang, S., Whitesides, G. M. & Ingber, D. E. Geometric control of cell life and death. *Science* **276,** 1425–1428 (1997).
9. Provenzano, P. P., Inman, D. R., Eliceiri, K. W. & Keely, P. J. Matrix density-induced mechanoregulation of breast cell phenotype, signaling and gene expression through a FAK-ERK linkage. *Oncogene* **28,** 4326–4343 (2009).
10. Olson, E. N. & Nordheim, A. Linking actin dynamics and gene transcription to drive cellular motile functions. *Nature Rev. Mol. Cell Biol.* **11,** 353–365 (2010).
11. Zhao, B. *et al.* Inactivation of YAP oncoprotein by the Hippo pathway is involved in cell contact inhibition and tissue growth control. *Genes Dev.* **21,** 2747–2761 (2007).
12. Fu, J. *et al.* Mechanical regulation of cell function with geometrically modulated elastomeric substrates. *Nature Methods* **7,** 733–736 (2010).
13. Miralles, F., Posern, G., Zaromytidou, A. I. & Treisman, R. Actin dynamics control SRF activity by regulation of its coactivator MAL. *Cell* **113,** 329–342 (2003).
14. Pan, D. The hippo signaling pathway in development and cancer. *Dev. Cell* **19,** 491–505 (2010).
15. Oka, T., Mazack, V. & Sudol, M. Mst2 and Lats kinases regulate apoptotic function of Yes kinase-associated protein (YAP). *J. Biol. Chem.* **283,** 27534–27546 (2008).
16. Lei, Q. Y. *et al.* TAZ promotes cell proliferation and epithelial-mesenchymal transition and is inhibited by the hippo pathway. *Mol. Cell. Biol.* **28,** 2426–2436 (2008).
17. Chen, Z., Friedrich, G. A. & Soriano, P. Transcriptional enhancer factor 1 disruption by a retroviral gene trap leads to heart defects and embryonic lethality in mice. *Genes Dev.* **8,** 2293–2301 (1994).
18. Makita, R. *et al.* Multiple renal cysts, urinary concentration defects, and pulmonary emphysematous changes in mice lacking TAZ. *Am. J. Physiol. Renal Physiol.* **294,** F542–F553 (2008).
19. Morin-Kensicki, E. M. *et al.* Defects in yolk sac vasculogenesis, chorioallantoic fusion, and embryonic axis elongation in mice with targeted disruption of *Yap65*. *Mol. Cell. Biol.* **26,** 77–87 (2006).
20. Skouloudaki, K. *et al.* Scribble participates in Hippo signaling and is required for normal zebrafish pronephros development. *Proc. Natl Acad. Sci. USA* **106,** 8579–8584 (2009).
21. Nienhaus, U., Aegerter-Wilmsen, T. & Aegerter, C. M. Determination of mechanical stress distribution in *Drosophila* wing discs using photoelasticity. *Mech. Dev.* **126,** 942–949 (2009).
22. Schwank, G. & Basler, K. Regulation of organ growth by morphogen gradients. *Cold Spring Harb. Perspect. Biol.* **2,** a001669 (2010).
23. Hong, J. H. *et al.* TAZ, a transcriptional modulator of mesenchymal stem cell differentiation. *Science* **309,** 1074–1078 (2005).

Supplementary Information is linked to the online version of the paper at www.nature.com/nature.

Acknowledgements We thank G. Scita for advice and gift of reagents; X. Yang for 5SA-YAP1 plasmid; I. Farrance for 4×GTIIC-lux plasmid; H. Miyoshi for pCSII-EF-MCS vector; L. Naldini for pMD2-VSVG vector; R. Treisman for ΔN1+C mDIA, R26D and V159N Actin plasmids; G. Posern for SRF-lux reporter; mouse TAZ and psPAX2 were Addgene plasmid 19025 and 12260. This work was supported by: Telethon and Progetti di Eccellenza CARIPARO grants to N.E.; AIRC (Italian Association for Cancer Research) PI and AIRC Special Program Molecular Clinical Oncology ''5 per mille'', University of Padua Strategic grant, IIT Excellence grant and Telethon to S.P.; AIRC PI and MIUR (Italian Minister of University) grants to S.D.

Author Contributions S.D., L.M. and S.P. designed research; L.M., S.D., M.A., E.E. and F.Z. performed experiments; M.C., S.B. and M.F. performed bioinformatics analysis; N.E. and S.G. prepared hydrogels; J.LeD. prepared micropost arrays; S.D. and S.P. coordinated the project; S.D. and S.P. wrote the manuscript.

Author Information Reprints and permissions information is available at www.nature.com/reprints. The authors declare no competing financial interests. Readers are welcome to comment on the online version of this article at www.nature.com/nature. Correspondence and requests for materials should be addressed to S.D. (dupont@bio.unipd.it) and S.P. (piccolo@bio.unipd.it).

METHODS

Reagents, microfabrications and plasmids. Cell-permeable C3 transferase (Cytoskeleton Inc.) was used in serum-free conditions for MCF10A and MSC, in complete medium for HMVEC. Y27632, blebbistatin, nocodazole were from Sigma. Latrunculin A was from Santa Cruz. NSC23766 was from Tocris. Micropatterned glass slides were purchased from Cytoo SA; on every slide, square islands of different sizes were arrayed in quadrants, leaving 70 μm of non-adhesive glass between each island; a control area evenly coated with fibronectin was also included to let cells attach without geometric constraints. Fibronectin-coated hydrogels were synthesized according to ref. 24. Micropost arrays were prepared according to ref. 25, with microposts of 1 μm in diameter and 3 μm of centre-to-centre distance; elasticity of the micropillars was changed by modulating the amount of cross-linker (10% in the stiff micropillars, 5% in the elastic ones) and their length, as in ref. 12, to obtain nominal spring constants of >10.9 nN μm^{-1} for rigid micropillars, and 1.39 nN μm^{-1} for the elastic ones. 5SA-YAP1 was subcloned into pCSII-EF-MCS to produce lentiviral particles. 4SA-mouse TAZ cDNA was synthesized ad hoc (GeneScript).

Cell lines, transfections and treatments. Mouse NMuMG cells were grown in DMEM 10% FCS. Human MCF10A cells were grown in DMEM/F12 with 5% horse serum freshly supplemented with insulin, epidermal growth factor, hydrocortisone and cholera toxin. Human MDA-MB-231 cells were grown in DMEM/F12 with 10% FBS. Bone marrow-derived MSC and HMVEC-L were purchased from Lonza and grown according to the manufacturer's instructions. siRNA transfections were done with Lipofectamine RNAi-MAX (Invitrogen) in antibiotics-free medium according to manufacturer's instructions. Sequences of siRNAs is provided in Supplementary Table 2. DNA transfections were done with TransitLT1 (Mirus Bio). Lentiviral particles were prepared by transiently transfecting HEK293T cells with lentiviral vectors together with packaging vectors (pMD2-VSVG and psPAX2). Luciferase assays with the established YAP/TAZ-responsive reporter 4×GTIIC-lux[26] were as in ref. [27], and displayed as arbitrary units.

For hydrogels, 5,000–10,000 cells per cm^2 were seeded in drop; after attachment, the wells containing the hydrogels were filled with appropriate medium. MSC and mammary cells were plated in growth medium and harvested for immunofluorescence after 24 h; for luciferase and gene expression after 48 h. For bone differentiation assays, growth medium was changed with osteogenic differentiation medium 24 h after seeding, and renewed every 2 days for a total of 8 days of differentiation. Bone differentiation was assayed by alkaline phosphatase staining (Sigma 85L2) and quantified with ImageJ software as follows: for each sample, at least five low magnification (×20) pictures were taken, and the alkaline-phosphatase-positive area was determined with ImageJ as the number of blue pixels across the picture; this value was then normalized to the number of cells (Hoechst/nuclei) for each picture (arbitrary units). For adipogenic differentiation, growth medium was replaced with adipogenic induction medium 24 h after seeding; cells were then subjected to cycles of 3 days of adipogenic induction and 1 day of adipogenic maintenance until harvesting at day 7 of differentiation. Adipogenic differentiation was assayed by Oil Red staining (Sigma) and quantified as the Oil Red-positive area normalized to the number of cells (Hoechst-positive nuclei) in a manner similar to that described for bone differentiation.

For micropatterns and micropost arrays, 40,000 HMVEC or MSC cells were plated in 35-mm dishes in growth medium. For immunofluorescence, cells were fixed 24 h after plating. For HMVEC proliferation and apoptosis assays, cells were fixed 24 h after plating (including 1 h incubation with BrdU in the case of proliferation assays) and processed according to TUNEL or BrdU detection kits (Promega DeadEnd and Roche Kit number 1, respectively). The projected cell area of cells on fibronectin-coated glass slides and on microposts was determined with imageJ based on immunofluorescence pictures of cells stained with anti-YAP/TAZ; the area of ECM contacted by cells was estimated by calculating that microposts (diameter 1 μm) arrayed in equilateral triangles (centre-to-centre 3 μm) approximate 10% of the total surface covered by cells (projected cell area).

For drug treatments and immunofluorescence, 10,000 cells per cm^2 were plated onto 8-well glass Lab-Tek chamberslides (Nunc) precoated for 1 h at 37 °C with 20 μg ml^{-1} bovine fibronectin (Sigma) in 1× PBS. Unless indicated otherwise, drug concentrations are indicated in the legend to Fig. 2a and d, and treatments lasted 4 h for immunofluorescence, 6 h for western blotting, and overnight for luciferase and gene expression assays. For serum stimulations, cells were incubated overnight without serum and then stimulated for 6 h with 20% serum; for combined treatments, drugs were added together with 20% serum.

Antibodies, western blotting and immunofluorescence. Western blotting was carried out as in ref. 28. Immunofluorescence was as in ref. 29. Antibodies: anti-YAP/TAZ 1:200 for immunofluorescence (sc101199 detecting both YAP and TAZ in western blot), anti-YAP 1:100 for immunofluorescence (sc271134 detecting only YAP in western blot, used in Supplementary Fig. 5), anti-phosphoS127-YAP (CST 4911), anti-LATS1 (CST 3477), anti-LATS2 (Abnova ab70565), anti-GAPDH (Millipore mAb374), anti-vinculin[30,31] (VIN-11-5). Primary antibodies for immunofluorescence were incubated overnight in PBS with 0.1% Triton and 2% goat serum. Secondary antibodies were GAM Alexa488, GAM Alexa568 and GAR Alexa555 (Invitrogen). YOYO1, TOTO3 (Invitrogen) or Hoechst were used in combination with RNase to counterstain nuclei. Alexa 488-conjugated phalloidin (Invitrogen) was used 1:100 in 1% BSA to visualize F-actin microfilaments. Firm-setting anti-fade mounting medium was 10% Mowiol 4-88, 2.5% DABCO, 25% glycerol, 0.1 M Tris-HCl pH 8.5. Images were acquired with a Leica SP2 confocal microscope equipped with a CCD camera. Cells seeded on microposts were observed in 1× PBS with a Bio-Rad upright confocal microscope with water immersion long-range objectives. Pictures of cells seeded on small adhesive islands were rescaled to allow better visualization of immunostainings. For quantifications of YAP/TAZ subcellular localizations, YAP/TAZ immunofluorescence signal was scored as predominantly nuclear versus evenly distributed/predominantly cytoplasmic in 150–200 cells for each experimental condition.

Real-time PCR. Cultures were harvested in TRIzol (Invitrogen) for total RNA extraction, and contaminant DNA was removed by DNase I treatment. cDNA synthesis was carried out with dT-primed MuMLV Reverse Transcriptase (Invitrogen). Real-time qPCR analyses were carried out on triplicate samplings of retrotranscribed cDNAs with RG3000 Corbett Research thermal cycler and analysed with Rotor-Gene Analysis6.1 software. Expression levels are given relative to *GAPDH*. Sequences of primers are provided in Supplementary Table 3.

Biostatistical analysis. The statistical association between genes differentially expressed in mammary epithelial cells (MEC) cultivated on ECM of high/low stiffness (stiffness signature) and belonging to signal transduction pathways is assessed by an over-representation analysis approach using Fisher's exact test. Briefly, considering that there are *S* single-symbol-annotated genes on the stiffness signature, the over-representation of a pre-defined pathway signature is calculated as the hypergeometric probability of having α genes for a specific pathway in *S*, under the null hypothesis that they were picked out randomly from the *N* total genes of the microarray. Over-representation analysis has been conducted using one-sided Fisher's exact test (*phyper* function of R *stats* package; *P*-value < 0.05) and considering 19,621 single-symbol-annotated genes on the HG-U133 Plus2.0 microarray. *P*-values have been adjusted for false discovery rate (*p.adjust* function of R *stats* package; FDR $< 5\%$).

The stiffness signature has been derived from Supplementary Table 1 of ref. 9. The complete signature contains 1,236 probe sets of the Affymetrix 430 2.0 mouse array accounting for 1,015 single-symbol-annotated. MOE430 Plus2.0 probe IDs have been converted to the correspondent HG-U133 Plus2.0 probe sets using the NetAffx orthologue annotation file derived from the NCBI HomologoGene database (MOE430A Orthologues/Homologues Release 30, http://www.affymetrix.com/). This conversion table allows mapping orthologous probe sets (that is, probe sets interrogating transcripts from orthologous genes) across two Affymetrix types of arrays. The 1,236 mouse probe sets of the stiffness signature were converted into 1,793 human probe sets corresponding to 807 single-symbol-annotated genes. Similarly, probe sets of all pathway signatures have been first converted into HG-U133 Plus2.0 probe sets, and then annotated as gene symbols using Bioconductor *hgu133plus2.db* package (release 2.3.5). Gene-sets of specific signalling pathways have been derived from: TGFβa[32]; TGFβb[33]; H-Ras and β-catenin[34]; ERBB2[35]; YAP[36–38]; YAP/TAZ[39]; WNT[40]; Notch and NICD[41]. The "YAP/TAZ signature" was published as supplemental table in ref. 39. The second "YAP signature" of Supplementary Fig. 2 is provided in Supplementary Table 1. See Supplementary Tables 4, 5 and 6 for the following signatures, that were derived from the microarrays published in: MAL/SRFa[42]; MAL/SRFb[43]; NF-κB[44]. Genes of WNT and β-Catenin pathway lists were not represented in the stiffness signature.

24. Tse, J. R. & Engler, A. J. Preparation of hydrogel substrates with tunable mechanical properties. *Curr. Protoc. Cell Biol.* **47,** 10.16.1–10.16.16 (2010).
25. du Roure, O. *et al.* Force mapping in epithelial cell migration. *Proc. Natl Acad. Sci. USA* **102,** 2390–2395 (2005).
26. Mahoney, W. M. Jr, Hong, J. H., Yaffe, M. B. & Farrance, I. K. The transcriptional co-activator TAZ interacts differentially with transcriptional enhancer factor-1 (TEF-1) family members. *Biochem. J.* **388,** 217–225 (2005).
27. Martello, G. *et al.* A MicroRNA targeting Dicer for metastasis control. *Cell* **141,** 1195–1207 (2010).
28. Dupont, S. *et al.* FAM/USP9x, a deubiquitinating enzyme essential for TGFβ signaling, controls Smad4 monoubiquitination. *Cell* **136,** 123–135 (2009).
29. Morsut, L. *et al.* Negative control of Smad activity by ectodermin/Tif1γ patterns the mammalian embryo. *Development* **137,** 2571–2578 (2010).
30. Galbraith, C. G., Yamada, K. M. & Sheetz, M. P. The relationship between force and focal complex development. *J. Cell Biol.* **159,** 695–705 (2002).
31. Giannone, G., Jiang, G., Sutton, D. H., Critchley, D. R. & Sheetz, M. P. Talin1 is critical for force-dependent reinforcement of initial integrin-cytoskeleton bonds but not tyrosine kinase activation. *J. Cell Biol.* **163,** 409–419 (2003).

32. Padua, D. *et al.* TGFβ primes breast tumors for lung metastasis seeding through angiopoietin-like 4. *Cell* **133,** 66–77 (2008).
33. Adorno, M. *et al.* A mutant-p53/Smad complex opposes p63 to empower TGFβ-induced metastasis. *Cell* **137,** 87–98 (2009).
34. Bild, A. H. *et al.* Oncogenic pathway signatures in human cancers as a guide to targeted therapies. *Nature* **439,** 353–357 (2006).
35. Mackay, A. *et al.* cDNA microarray analysis of genes associated with *ERBB2* (HER2/*neu*) overexpression in human mammary luminal epithelial cells. *Oncogene* **22,** 2680–2688 (2003).
36. Zhao, B. *et al.* TEAD mediates YAP-dependent gene induction and growth control. *Genes Dev.* **22,** 1962–1971 (2008).
37. Dong, J. *et al.* Elucidation of a universal size-control mechanism in *Drosophila* and mammals. *Cell* **130,** 1120–1133 (2007).
38. Ota, M. & Sasaki, H. Mammalian Tead proteins regulate cell proliferation and contact inhibition as transcriptional mediators of Hippo signaling. *Development* **135,** 4059–4069 (2008).
39. Zhang, H. *et al.* TEAD transcription factors mediate the function of TAZ in cell growth and epithelial-mesenchymal transition. *J. Biol. Chem.* **284,** 13355–13362 (2009).
40. DiMeo, T. A. *et al.* A novel lung metastasis signature links Wnt signaling with cancer cell self-renewal and epithelial-mesenchymal transition in basal-like breast cancer. *Cancer Res.* **69,** 5364–5373 (2009).
41. Mazzone, M. *et al.* Dose-dependent induction of distinct phenotypic responses to Notch pathway activation in mammary epithelial cells. *Proc. Natl Acad. Sci. USA* **107,** 5012–5017 (2010).
42. Descot, A. *et al.* Negative regulation of the EGFR-MAPK cascade by actin-MAL-mediated Mig6/Errfi-1 induction. *Mol. Cell* **35,** 291–304 (2009).
43. Selvaraj, A. & Prywes, R. Expression profiling of serum inducible genes identifies a subset of SRF target genes that are MKL dependent. *BMC Mol. Biol.* **5,** 13 (2004).
44. Park, B. K. *et al.* NF-κB in breast cancer cells promotes osteolytic bone metastasis by inducing osteoclastogenesis via GM-CSF. *Nature Med.* **13,** 62–69 (2006).